IEEE Access
Multidisciplinary | Rapid Review | Open Access Journal

Received January 5, 2021, accepted January 12, 2021, date of publication January 18, 2021, date of current version January 27, 2021.

Digital Object Identifier 10.1109/ACCESS.2021.3052558

Third Harmonic Current Injection in Different Operating Stages of Five-Phase PMSM With Hybrid Single/Double Layer Fractional-Slot Concentrated Winding

JIAXUAN HUANG[1], PING ZHENG[1], (Senior Member, IEEE), YI SUI[1], (Member, IEEE), JIGUI ZHENG[2], ZUOSHENG YIN[1], AND LUMING CHENG[1]

[1]School of Electrical Engineering and Automation, Harbin Institute of Technology, Harbin 150080, China
[2]Beijing Institute of Precise Mechatronics and Controls, Beijing 100000, China

Corresponding authors: Ping Zheng (zhengping@hit.edu.cn) and Yi Sui (suiyi_hitee2005@163.com)

This work was supported in part by the National Natural Science Foundation of China under Grant 51991385, Grant 51521003, Grant 51977048, and Grant 51777013; and in part by the Fundamental Research Funds for the Central Universities under Grant HIT. NSRIF.201811.

ABSTRACT In this paper, 30-slot/24-pole five-phase PMSM with hybrid single/double layer (HL) fractional-slot concentrated winding (FSCW) is designed for wheel-driving application in electric vehicles (EVs). Third harmonic current injection in different operating stages of the machine is investigated, including normal operation and fault-tolerant operation. HL FSCW machine is validated to be suitable for injecting third harmonic current to enhance torque by both theoretical analysis and finite-element analysis (FEA), and compared with 20-slot/24-pole single-layer (SL) and double-layer (DL) FSCW machine under constant rms and peak harmonic injection. Besides, a novel flux weakening control method with third harmonic current injection is proposed, which improves torque and efficiency of HL FSCW machine. The influence of nonlinearity caused by stator core saturation and higher order harmonics contained in back electromotive force (EMF) is included in flux weakening operation with harmonic injection. Finally, fault-tolerant control of HL FSCW machine with one-phase open-circuit fault is investigated, and two compensatory strategies with and without third harmonic current injection are proposed. Torque ripple caused by one-phase open-circuit fault is suppressed effectively by the proposed strategies.

INDEX TERMS Permanent-magnet synchronous machine (PMSM), five-phase, fractional-slot concentrated winding (FSCW), third harmonic injection, flux weakening, fault-tolerant control, open-circuit.

I. INTRODUCTION

Compared with three-phase permanent-magnet synchronous machines (PMSMs), multiphase PMSMs with fractional-slot concentrated winding (FSCW) have advantages of high fault-tolerant capacity and more control freedom because of the increase of phase number [1], [2]. Owing to the inherent advantages, multiphase FSCW PMSMs receive more and more attention in safety-crucial applications of electric vehicle (EV), marine propulsion, and more-electric aircraft nowadays [3]–[5]. Besides, torque density of multiphase FSCW PMSM can be improved by harmonic current injection, which makes it more favorable in high torque density demanding cases [6]. Five-phase brushless permanent-magnet (PM) machine with trapezoidal back electromotive force (EMF) supplied by third harmonic current injection achieves better performance compared with both brushless dc machine and PMSM, due to vector decoupling control of d_1-q_1 and d_3-q_3 harmonic space [7]. With constant rms harmonic injection, nine-phase machine with PM whose pole arc coefficient is only 0.389 generates almost the same torque compared with machine with full-pitch PM [8], [9]. The optimal injection ratio of harmonic current for maximizing output torque of multiphase machine has been analyzed, which is related with the ratio of the corresponding harmonics contained in the back EMF of multiphase PMSM [9], [10].

The associate editor coordinating the review of this manuscript and approving it for publication was Agustin Leobardo Herrera-May.

Many researches focus on the design of multiphase PMSM to maximize torque with harmonic injection, and five-phase PMSMs have been researched the most. A five-phase PMSM with unequal teeth is designed to enhance both the fundamental and the third harmonic contained in back EMF, which improves torque with third harmonic current injection [11]–[15]. A novel 15-slot/12-pole modular five-phase PMSM with hybrid single/double layer (HL) FSCW is proposed in [16], which also improves the fundamental and the third harmonic contained in back EMF. An optimal winding configuration design method for maximizing torque of multiphase machine with arbitrary phase numbers under harmonic injection is proposed in [17], which optimizes winding factors of harmonics contained in back EMF. Apart from optimization of stator core and winding configuration, optimization of the shape of PM is also researched for torque enhancement of five-phase PMSM with harmonic current injection, including segmented PM and harmonic-shaped PM [13]–[15]. To summarize, different novel machine topologies are designed to realize the aim of improving output torque with harmonic injection, and machine performance under healthy condition has been investigated extensively. However, fault-tolerant performance of five-phase PMSM specially designed for harmonic injection has not been deeply researched. Fault-tolerant strategies for five-phase machine with open-circuit fault are proposed under the constraints of the unchanged magnetomotive force (MMF) or the minimal copper loss, which suppresses torque ripple under fault condition effectively [18], [19]. However, most fault-tolerant strategies are not suitable for machine with high third harmonic in back EMF, since only the fundamental harmonic in back EMF is taken into account in the derivation of compensatory currents. Although some fault-tolerant strategies are proposed to address the negative impact of third harmonic in back EMF on fault-tolerant operation of five-phase PMSM [20]–[22], compensation effect of fault-tolerant strategies is deteriorated due to the ignorance of harmonics in back EMF whose orders are higher than 3.

Except from torque improvement, third harmonic current injection is also applied to flux weakening operation of five-phase PMSM. Flux weakening is proposed for three-phase PMSM operating at high speed [23], which is also extended to multiphase PMSM. Vector decoupling method is used to regulate both the fundamental and the third harmonic current of five-phase PMSM at flux weakening region [24], [25]. During flux weakening operation, phase angle of the third harmonic current is directly kept to be three times of that of the fundamental current in [25]. Although the phase voltage of five-phase machine is controlled to satisfy the limit of DC-link voltage, the relation of the first and third harmonic in phase voltage is not taken into consideration [25]. A novel bi-harmonic five-phase PMSM with double p/3p polarity is proposed in [26]–[29], and the third harmonic current is applied to the bi-harmonic five-phase PMSM during flux weakening process to reduce the amplitude of phase voltage [27]–[29]. Compared with three-phase PMSM, bi-harmonic five-phase PMSM produces higher torque, and has larger speed range during flux weakening operation [27]. Franck Scuiller extends the method of injecting third harmonic current during flux weakening process to five-phase machine with only one polarity. A simplified numerical calculation method based on the analysis of inductance and back EMF is proposed to estimate performance of five-phase PMSM at flux weakening region [30], [31]. However, few researches deal with the nonlinearity caused by armature reaction and higher order harmonics contained in back EMF (including the 5^{th} harmonic and so on), which also influences the torque/speed characteristics at flux weakening region with third harmonic current injection.

In this paper, third harmonic current injection in different operating stages of five-phase HL FSCW machine is investigated, including normal operation and fault-tolerant operation. In section II, 30-slot/24-pole five-phase HL FSCW machine is designed for wheel-driving application in EVs. In section III, HL FSCW machine is validated to be suitable for third harmonic current injection to enhance torque, and compared with conventional 20-slot/24-pole SL and DL FSCW machine. Then, third harmonic current is injected to HL FSCW machine for flux weakening operation, and the influence of nonlinearity caused by saturation in stator core and higher order harmonics contained in back EMF is taken into consideration by finite-element analysis (FEA), in section IV. Finally, for HL FSCW machine with one-phase open-circuit fault, two compensatory strategies, with and without third harmonic current injection, are proposed in section V, which suppresses the negative impact of higher order harmonics contained in back EMF on fault-tolerant performance.

II. DESIGN OF 30-SLOT/24-POLE HL FSCW MACHINE

30-slot/24-pole five-phase HL FSCW machine is designed for wheel-driving application in EVs, and compared with 20-slot/24-pole single-layer (SL) FSCW machine and 20-slot/24-pole double-layer (DL) FSCW machine. Structures of different machines are shown in Fig. 1. SL, DL, and HL FSCW machine are designed under the same specifications to ensure a fair comparison, as listed in Table 1.

30-slot/24-pole HL FSCW machine is transformed from 20-slot/24-pole DL FSCW machine. Redundant non-wound teeth are added to DL FSCW machine, and double-layer slots (DLSs) with coils from different phases are separated to two single-layer slots (SLSs), as illustrated in Fig. 1. DLSs with coils belonging to the same phase remain unchanged. Therefore, compared with DL FSCW machine, slot number of HL FSCW machine is increased from 20 to 30, since 10 DLSs in DL FSCW machine are changed into 20 SLSs in HL FSCW machine. Three-dimensional (3-D) model of HL FSCW machine is shown in Fig. 2, and modular production is achieved by HL FSCW machine, which means that HL FSCW machine can be assembled by 10 modular cores through round-shape joints.

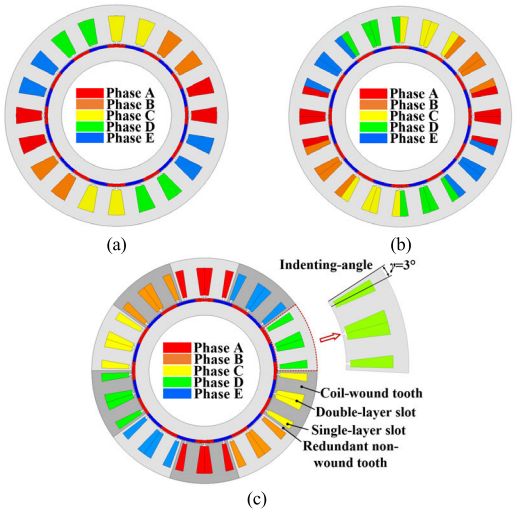

FIGURE 1. Machine structure. (a) 20-slot/24-pole SL FSCW machine; (b) 20-slot/24-pole DL FSCW machine; (c) 30-slot/24-pole HL FSCW machine.

TABLE 1. Specifications of HLFSCW machine.

Specifications	Units	Values
Rated power	kW	11
Rated speed	rpm	500
Maximum power	kW	16
Maximum speed	rpm	1400
DC-link voltage	V	500
Material of PMs	-	N52H (B_r=1.32T)
Stator outer diameter	mm	325
Stator inner diameter	mm	210
Rotor inner diameter	mm	160
Air-gap length	mm	1
Stack length	mm	100
Pole arc coefficient	-	1
Magnet height	mm	4
No. of conductors per slot [1]	-	80
Slot fill factor [2]	%	74.37/72.81

[1]For HL FSCW machine, number of conductors per double-layer slot is 80, whereas number of conductors per single-layer slot is 40.
[2]The slot fill factor of DL and HL FSCW machine are 74.37%, and the slot fill factor of SL FSCW machine is 72.81%.

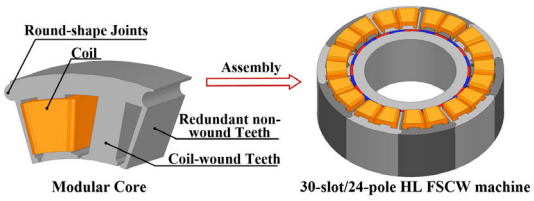

FIGURE 2. Three-dimensional (3-D) model of HL FSCW machine.

For further analysis of HL FSCW machine, indenting-angle (γ) is introduced, which indicates the angle between SLS and redundant non-wound tooth, as shown in Fig. 1(c). Theory of winding function is applied to analyze the synthesized MMF of HL FSCW machine, which is based on the assumption that the permeability of stator core is infinite ($\mu_{\mathrm{Fe}} \to \infty$), and the current in each slot is concentrated in the center of the slot. Winding function of Phase-A in HL FSCW machine ($N_{\mathrm{A}}(\theta_{\mathrm{m}})$) is shown in red lines in Fig. 3.

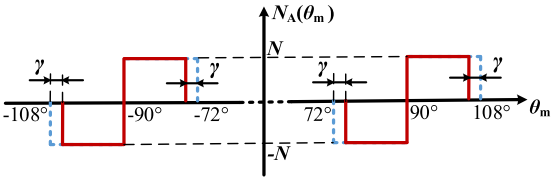

FIGURE 3. Winding function of Phase-A in 30-slot/24-pole HL FSCW machine.

Fourier expansion of $N_{\mathrm{A}}(\theta_{\mathrm{m}})$ is expressed by (1).

$$\begin{cases} N_{\mathrm{A}}(\theta_{\mathrm{m}}) = \sum_{k=1}^{\infty} a_k \sin(k\theta_{\mathrm{m}}) \\ a_k = \frac{2}{\pi}\left[\int_{72^\circ+\gamma}^{90^\circ} -N\cdot\sin(k\theta_{\mathrm{m}})d\theta_{\mathrm{m}} + \int_{90^\circ}^{108^\circ-\gamma} N\cdot\sin(k\theta_{\mathrm{m}})d\theta_{\mathrm{m}}\right] \\ \quad = \frac{8N}{k\pi}\xi_{wk} \\ \xi_{wk} = \frac{1}{2}\cos(\frac{k\pi}{2})\left\{1-\cos\left[k\left(\frac{\pi}{10}-\gamma\right)\right]\right\} \end{cases} \tag{1}$$

where N is turns-in-series per-coil; k is the order of the harmonic; ξ_{wk} is the winding factor of the k^{th} harmonic. It is worth to mention that the winding function of Phase-A in DL FSCW machine can be represented by (1) when $\gamma = 0°$, whereas the winding function of Phase-A in HL FSCW machine is represented by (1) when $\gamma > 0°$.

The MMF of Phase-A in HL FSCW machine and the MMF synthesized by all five phases are expressed by (2) and (3), respectively.

$$F_{\mathrm{A}} = N_{\mathrm{A}}(\theta_{\mathrm{m}})\cdot i_{\mathrm{A}} = \sum_{k=1}^{\infty} a_k \sin(k\theta_{\mathrm{m}})\cdot I\sin(\omega_e t) \tag{2}$$

$$\begin{aligned} \mathrm{MMF} &= F_{\mathrm{A}} + F_{\mathrm{B}} + F_{\mathrm{C}} + F_{\mathrm{D}} + F_{\mathrm{E}} \\ &= \begin{cases} \sum_{k=1}^{\infty} \frac{20NI}{\pi k}\xi_{wk}\cos(k\theta_m + \omega_e t) & k = 10n-2 \\ \sum_{k=1}^{\infty} \frac{20NI}{\pi k}\xi_{wk}\cos(k\theta_m - \omega_e t) & k = 10n+2 \end{cases} \end{aligned} \tag{3}$$

where I is the amplitude of phase current; ω_e is the electrical angular velocity; n is a positive integer. It is found in (3) that different harmonics whose orders satisfy (10n±2) are contained in the synthesized MMF, and the amplitude of each harmonic is proportional to the corresponding winding factor. Since ξ_{wk} is influenced by γ, the winding factor of the working harmonic (the 12^{th} harmonic) can be improved, and the winding factors of other non-working harmonics can be suppressed by optimizing γ. When γ changes from 0° to 6°, the winding factors of the 2^{nd} and 8^{th} harmonic decrease monotonously, as shown in Fig. 4. Conversely, the winding

TABLE 2. Winding factor comparison.

Winding configuration	ξ_{w2}	ξ_{w8}	ξ_{w12}	ξ_{w18}	ξ_{w22}	ξ_{w28}	ξ_{w32}
SL FSCW	0.309	0.951	0.951	0.309	0.309	0.951	0.951
DL FSCW	0.095	0.905	0.905	0.095	0.095	0.905	0.905
HL FSCW	0.067	0.75	1	0.5	0.067	0.25	0.75

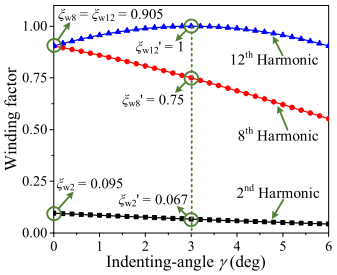

FIGURE 4. The winding factors of different harmonics during the variation of indenting-angle (γ).

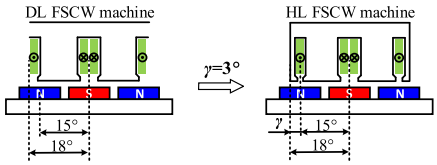

FIGURE 5. Transformation from 20-slot/24-pole DL FSCW machine to 30-slot/24-pole HL FSCW machine.

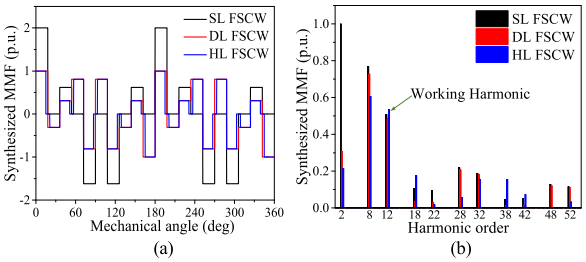

FIGURE 6. Synthesized MMF of SL, DL, and HL FSCW machine derived from theoretical analysis. (a) Waveforms; (b) Harmonic analysis.

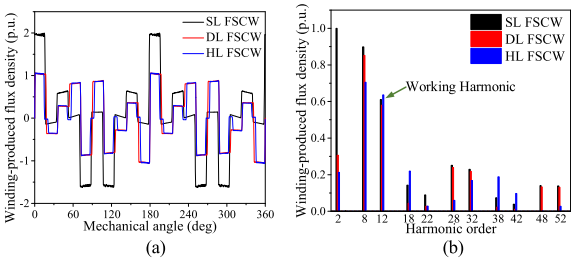

FIGURE 7. Winding-produced air-gap flux density of SL, DL, and HL FSCW machine derived from FEA. (a) Waveforms; (b) Harmonic analysis.

factor of the working harmonic reaches the maximum of 1 when γ equates to 3°, so γ is chosen to be 3° to design HL FSCW machine. From another aspect, compared with DL FSCW machine, the coil-pitch of HL FSCW machine decreases from 18° to (18°-γ), as shown in Fig. 5. Since the coli-pitch of HL FSCW machine is equal to the pole-pitch when γ is 3°, the winding factor of the working harmonic is increased.

Winding factors of different harmonics in the synthesized MMF of SL, DL, and HL FSCW machine are listed in Table 2. The winding factor of the 12th harmonic (ξ_{w12}) in HL FSCW machine is higher than that of both SL and DL FSCW. The winding factor of the 2nd harmonic (ξ_{w2}) and the 8th harmonic (ξ_{w8}) in HL FSCW machine decrease, both lower than those of SL and DL FSCW machine.

The synthesized MMF of SL, DL, and HL FSCW machine are shown in Fig. 6(a), which is derived from theoretical analysis. Harmonic analysis of the synthesized MMF is shown in Fig. 6(b), and the amplitudes of different harmonics consist with the corresponding winding factor. Then, to verify the theoretical analysis of the synthesized MMF, winding-produced air-gap flux density of SL, DL, and HL FSCW machine are obtained through FEA as shown in Fig. 7, which is consistent with the synthesized MMF. More details about finite element method (FEM) used for analyses of SL, DL, and HL FSCW machine are in the Appendix A.

Apart from the 2nd, 8th, and 12th harmonic mentioned before, the amplitudes of other harmonics (including the 18th harmonic and so on) contained in the MMF of HL FSCW machine are also changed due to the change of winding configuration, which can be seen in Fig. 6. The increase of the working harmonic leads to the increase of average torque, and the suppress of non-working harmonics reduces the saturation of stator core and decreases PM loss (eddy current loss of PMs). However, although the amplitudes of harmonics whose orders are lower than the working harmonic (including the 2nd and the 8th harmonic) are reduced, the amplitudes of some harmonics whose orders are higher than the working harmonic, such as the 18th and 38th harmonic, are increased, which has negative impacts on machine performance. To evaluate the influence of different harmonics on machine performance, torque and PM loss of HL FSCW machine are analyzed as shown in Fig. 8. When the amplitude of phase current (including only the fundamental current) increases from 2.5A to 25A, torque of HL FSCW machine is constantly higher than that of SL and DL FSCW machine, which is because the amplitude of the working harmonic in the MMF of HL FSCW machine is higher than that of SL and DL FSCW machine. PM loss is only related with non-working harmonics in MMF, since the working harmonic rotates synchronously with the rotor and has no contribution to PM loss. Although some higher order non-working harmonics in the MMF of HL FSCW machine are higher

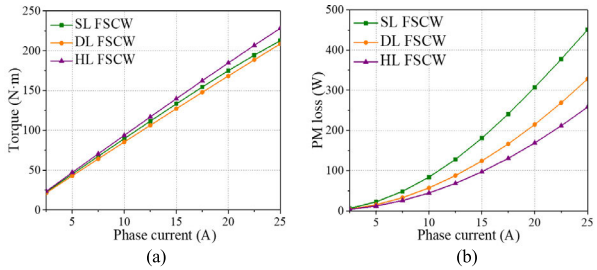

FIGURE 8. Average torque and PM loss of SL, DL, and HL FSCW machine during the variation of phase current. (a) Average torque; (b) PM loss.

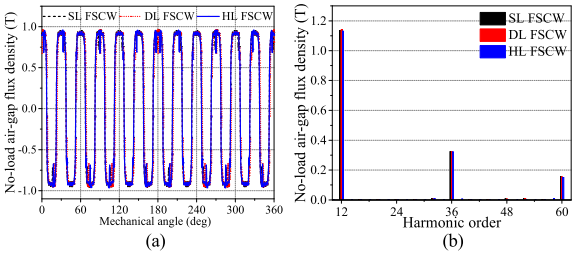

FIGURE 9. No-load air-gap flux density of SL, DL, and HL FSCW machine derived from FEA. (a)Waveforms; (b) Harmonic analysis.

than those of SL and DL FSCW machine, PM loss of HL FSCW machine is still lower than that of SL and DL FSCW machine, which is owing to the decrease of the 2nd and 8th harmonic in the MMF of HL FSCW machine. Therefore, since the amplitudes of harmonics whose orders are higher than the working harmonic are relatively lower, they have much less influence on machine performance than lower order harmonics including the 2nd and 8th harmonic.

No-load air-gap flux density of SL, DL, and HL FSCW machine are shown in Fig. 9(a), which is derived from FEA. Fourier expansion of no-load air-gap flux density ($B_{\mathrm{no-load}}$) is expressed in (4).

$$B_{\text{no-load}} = \sum B_k \cos(k\theta_{\mathrm{m}} \quad k = (2n-1)\,p \tag{4}$$

where k is the order of harmonic; p is the number of pole-pairs; θ_{m} is the mechanical angle; B_k is the amplitude of the k^{th} harmonic contained in $B_{\mathrm{no-load}}$. Harmonic analysis of no-load air-gap flux density of different machines are shown in Fig. 9(b), and the orders of harmonics contained in no-load air-gap flux density satisfy (4). Since pole arc coefficient is chosen to be 1 for all the machines, apart from the 12th harmonic, relatively high 36th and 60th harmonic are contained in the no-load air-gap flux density.

Back EMF of different machines at the rated speed of 500rpm are shown in Fig. 10(a), which is carried out by FEA. Harmonic analysis of back EMF is shown in Fig. 10(b), and the amplitude of the fundamental harmonic in back EMF of HL FSCW machine is higher than that of SL and DL FSCW machine. It is worth to note that the 3rd harmonic in back EMF of HL FSCW machine is also the highest, which means that HL FSCW machine is more suitable for third harmonic current injection to enhance torque than SL and DL machine.

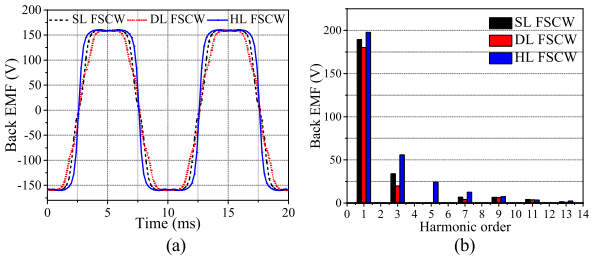

FIGURE 10. Back EMF of SL, DL, and HL FSCW machine at 500rpm derived from FEA. (a)Waveforms; (b) Harmonic analysis.

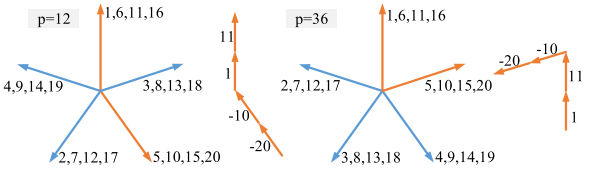

FIGURE 11. Star of slots of 20-slot/24-pole SL FSCW machine.

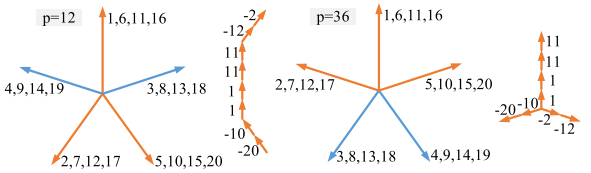

FIGURE 12. Star of slots of 20-slot/24-pole DL FSCW machine.

III. THIRD HARMONIC CURRENT INJECTION OF HL FSCW FIVE-PHASE MACHINE FOR TORQUE IMPROVEMENT

Third harmonic current is injected to SL, DL, and HL FSCW machine for torque improvement under normal operating condition. The injected third harmonic current interacts with the third harmonic in back EMF of five-phase machine to generate torque, which results in torque improvement compared with generating torque with only fundamental current. Torque generated by third harmonic current is calculated in (5),

$$T_3 = \frac{5E_3I_3}{2\omega_m} \tag{5}$$

where T_3 is the torque generated by third harmonic current injection; E_3 is the amplitude of the third harmonic in back EMF; I_3 is the amplitude of the third harmonic current; ω_m is the mechanical angular velocity. It can be found from (5) that the torque generated by third harmonic current injection is determined by E_3 in the case of a certain value of I_3. The higher E_3 means the higher torque generated by a certain value of I_3, namely higher utilization rate of third harmonic current. Since the rotor and turns-in-series per-phase of SL, DL, and HL FSCW machine are same, E_3 of each type of machine is only related to the winding factor of the 36th harmonic.

Star of slots is used to analyze the relationship of winding factor of the 12th and 36th harmonic of SL, DL, and HL FSCW machine, as shown in Fig. 11, Fig. 12, and Fig. 13. Slot potentials of different machines are represented by blue and orange vectors, and orange vectors belong to Phase-A of each

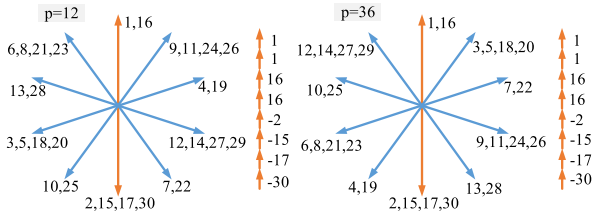

FIGURE 13. Star of slots of 30-slot/24-pole HL FSCW machine.

TABLE 3. Winding factor comparison.

Winding configuration	ξ_{w12}	ξ_{w36}
SL FSCW	0.951	0.588
DL FSCW	0.905	0.345
HL FSCW	1	1

type of machine. The length and the rotation angle of each vector represent the amplitude and the phase angle of each slot potential, respectively. Because of the addition of redundant non-wound teeth and the reduction of coil-pitch, star of slots of HL FSCW machine is different from that of SL and DL FSCW machine. The angle between each vector is 72° in star of slots of both SL and DL FSCW machine, whereas the angle between each vector is 36° of HL FSCW machine. Comparing Fig. 12 and Fig. 13, it is noticeable that when vectors belong to Phase-A are synthesized in the 12th and 36th harmonic space, the length of orange vectors in Fig. 12 is equal to the length of orange vectors in Fig. 13. However, the length of orange vectors in Fig. 11 is twice as long as orange vectors in Fig. 12 and Fig. 13, when vectors are synthesized in the 12th and 36th harmonic space. It is because turns-in-series per-coil of DL and HL FSCW machine is half than that of SL FSCW machine, which aims to keep turns-in-series per-phase of SL, DL, and HL FSCW machine equal.

It can be seen from Fig. 13 that the vector synthesized by orange vectors of HL FSCW machine in the 36th harmonic space is equal to the vector synthesized in the 12th harmonic space. So winding factor of the 36th harmonic is equal to that of the 12th harmonic in HL FSCW machine. Further, the synthesized vector in the 36th harmonic space of HL FSCW machine is longer than that of both SL and DL FSCW machine, as shown in Fig. 11 and Fig. 12. Thus, the winding factor of the 36th harmonic in HL FSCW machine is higher than that of SL and DL FSCW machine. Winding factor of the 12th and 36th harmonic of SL, DL, and HL FSCW machine are listed in Table 3, which consists with the analysis of star of slots.

Using FEA to verify the above-mentioned theoretical analysis, third harmonic current with the amplitude of 10A is injected to SL, DL, and HL machine. Torque of different machines are shown in Fig. 14, which is generated only by the third harmonic current. Torque of SL and DL FSCW machine is 59.33% and 35.90% of that of HL FSCW machine, which is identical with the proportion of winding factor of the 36th harmonic between SL, DL, and HL FSCW machine.

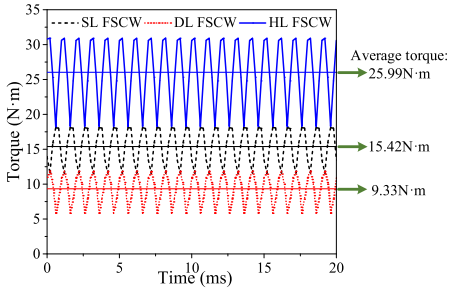

FIGURE 14. Torque generated by the third harmonic current.

For five-phase machine operating with third harmonic current injection, a certain ratio third harmonic current is injected and torque is generated by both fundamental current and the third harmonic current. In this paper, the optimal injection ratio of third harmonic current under constraints of constant rms and peak value of phase current is calculated according to the relation proposed in [10], which is expressed by (6) and (7),

$$R_{rms} = \frac{E_3}{E_1} \tag{6}$$

$$R_{peak} = \frac{1}{6 - 3\left(E_3/E_1\right)} \tag{7}$$

where E_1 is the amplitude of the fundamental back EMF; R_{rms} is the optimal injection ratio of third harmonic current under the constraint of constant rms value of phase current; R_{peak} is the optimal injection ratio of third harmonic current under the constraint of constant peak value of phase current. It has been proved in [10] that maximum torque is generated by keeping injection ratio of third harmonic current as (6) for constant rms harmonic injection. Similarly, maximum torque is generated by keeping injection ratio of third harmonic current equal to (7) for constant peak harmonic injection. Fundamental current and the third harmonic current of constant rms and peak harmonic injection are expressed by (8) and (9) [10],

$$\begin{cases} I_1 = \sqrt{\dfrac{1}{1 + R_{rms}^2}} I_0 \\ I_3 = R_{rms} I_0 \end{cases} \tag{8}$$

$$\begin{cases} I_1 = \dfrac{I_0}{8R_{peak}} \left(\dfrac{1 + 3R_{peak}}{12R_{peak}}\right)^{-1.5} \\ I_3 = R_{peak} I_0 \end{cases} \tag{9}$$

where I_1 is the amplitude of fundamental current; I_0 is the amplitude of phase current before third harmonic current injection.

Torque of SL, DL, and HL FSCW machine with optimal third harmonic current injection under constraints of constant rms and peak value of phase current (25A) are evaluated using FEA. The current density of SL, DL, and HL FSCW machine with constant rms and peak harmonic injection are listed in Table 4. Aiming to ensure a fair comparison of electromagnetic performance, current density is kept to be 4.29 A/mm^2 and 5.02 A/mm^2 among different machines under constant

TABLE 4. Current density of different machines.

case	SL FSCW Machine (A/mm^2)	DL FSCW Machine (A/mm^2)	HL FSCW Machine (A/mm^2)
(a) [1]	4.29	4.29	4.29
(b) [2]	5.03	5.02	5.02

[1]Case (a): Harmonic injection under constraint of constant rms value of phase current (25A). [2]Case (b): Harmonic injection under constraint of constant peak value of phase current (25A).

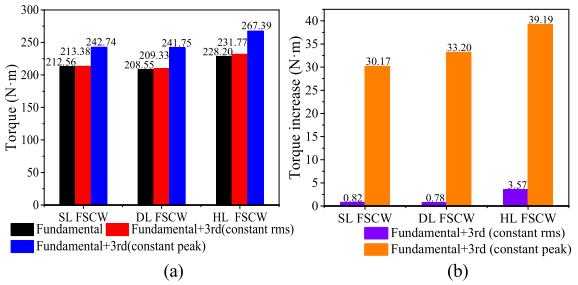

FIGURE 15. (a)Torque of different machines after third harmonic current injection; (b) Torque increase of different machines after third harmonic current injection.

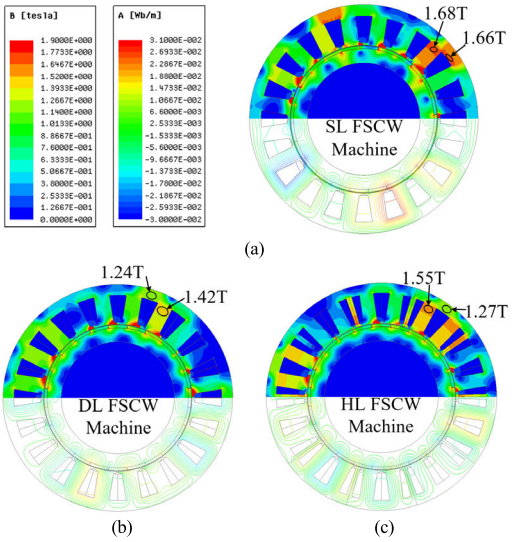

FIGURE 16. Flux density distributions and flux lines of different machines with harmonic injection under the constraint of constant rms value of phase current (25A). (a) SL FSCW machine; (b) DL FSCW machine; (c) HL FSCW machine.

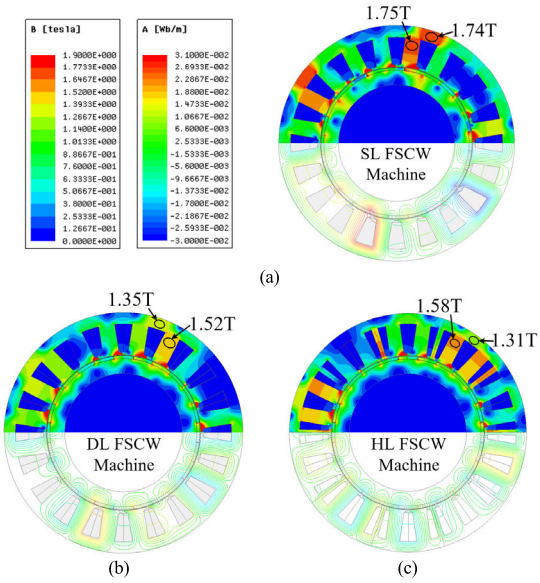

FIGURE 17. Flux density distributions and flux lines of different machines with harmonic injection under the constraint of constant peak value of phase current (25A). (a) SL FSCW machine; (b) DL FSCW machine; (c) HL FSCW machine.

rms and peak harmonic injection, respectively. For each type of machine, current density of constant rms harmonic injection is lower than that of constant peak harmonic injection. It is because the rms value of phase current is unchanged for constant rms harmonic injection compared with injecting only fundamental current, whereas the rms value of phase current is increased for constant peak harmonic injection.

Superior to injecting only fundamental current, output torque of different machines are improved by third harmonic current injection as shown in Fig. 15(a). Torque generated by constant peak harmonic injection is much higher than torque generated by constant rms harmonic injection. For constant rms harmonic injection, since the rms value of phase current is kept to be unchanged before and after third harmonic current injection, the amplitude of the fundamental current is actually reduced after harmonic injection, which can be found from (7). Thus, the torque increase of constant rms harmonic injection is brought by third harmonic current after complementing the torque loss caused by the decrease of fundamental current. However, since the amplitude of phase current needs to be unchanged for constant peak harmonic injection, the amplitude of the fundamental current and the rms value of phase current are both increased after harmonic injection. Therefore, torque is generated by not only the third harmonic current, but also by the fundamental current with a rising amplitude for constant peak harmonic injection.

Torque of HL FSCW machine with constant rms and peak harmonic injection are both higher than SL and DL FSCW machine, as shown in Fig. 15(a). Torque increase of SL and DL FSCW machine with constant rms harmonic injection are 0.82 N·m and 0.78 N·m, respectively, which is much lower than that of HL FSCW machine (3.57 N·m), as shown in Fig. 15(b). Besides, torque increase of HL FSCW machine with constant peak harmonic injection is 129.90% and 118.04% of that of SL and DL FSCW machine.

Magnetic field distributions of different machines with third harmonic current injection under constraints of constant rms and peak value of phase current (25A) are shown in Fig. 16 and Fig. 17, respectively. Flux density in the stator core of different machines are positively associated with the MMF synthesized by phase currents, which means that higher amplitudes of harmonics in MMF lead to higher flux density in stator core. As analyzed in section II, lower order harmonics in MMF (including the 2nd and 8th harmonic) have more influence on machine performance than higher order harmonics (including the 18th harmonic and so on). Since the amplitudes of the 2nd and 8th harmonic in the

MMF of SL FSCW machine are higher than those of DL and HL FSCW machine, flux density in the stator core of SL FSCW machine is higher than that of DL and HL FSCW machine under constant rms and peak harmonic injection, as shown in Fig. 16 and Fig. 17. Thus, the stator core of SL FSCW machine is more saturated due to higher flux density, compared with DL and HL FSCW machine. Besides, since torque generated by constant peak harmonic injection is higher than constant rms harmonic injection, stator cores of all machines are more saturated when applying constant peak harmonic injection, compared with constant rms harmonic injection.

Thus, through both theoretical analysis and FEA, HL FSCW machine is proved to be more suitable than SL and DL FSCW machine to enhance output torque by third harmonic current injection.

Further comparison of electromagnetic performance between SL, DL, and HL FSCW machine with constant rms and peak harmonic injection is conducted by FEA when I_0 changing form 2.5A to 25A. During the variation of I_0, torque of HL FSCW machine generated by constant rms harmonic injection (c_rms) and constant peak harmonic injection (c_peak) is higher than that of both SL and DL FSCW machine, as shown in Fig. 18(a). However, torque ripple of HL FSCW machine with constant rms and peak harmonic injection are also higher than torque ripple of SL and DL FSCW machine, as can be seen in Fig. 18(b).

For each type of machine, PM loss of constant peak harmonic injection is higher than that of constant rms harmonic injection, as shown in Fig. 18(c). For constant rms harmonic injection, PM loss of HL FSCW machine is similar with that of DL FSCW machine, and lower than PM loss of SL FSCW machine. For constant peak harmonic injection, PM loss of HL FSCW machine is lower than that of both SL and DL FSCW machine during the variation of I_0.

Similar with PM loss, core loss (including both stator core loss and rotor core loss) of each type of machine under constant peak harmonic injection is also higher than that of constant rms harmonic injection, as shown in Fig. 18(d). Core loss of HL FSCW machine is higher than that of DL FSCW machine during the variation of I_0 from 2.5A to 25A for both constant rms and peak harmonic injection. Conversely, core loss of HL FSCW machine with constant rms and peak harmonic injection becomes lower than that of SL FSCW machine when I_0 exceeds a certain value. Comparing core loss and PM loss, core loss becomes much lower than PM loss for each type of machine under constant rms and peak harmonic injection with the increase of I_0. It is because stator and rotor cores of all machines are stacked by silicon steel sheets to reduce eddy current loss, whereas the surface-mounted PMs in machines are not segmented.

It is noticeable from Fig. 18(c) and Fig. 18(d) that, when changing from constant rms harmonic injection to constant peak harmonic injection, the increase of PM loss and core loss of HL FSCW machine are much less than those of SL and DL FSCW machine.

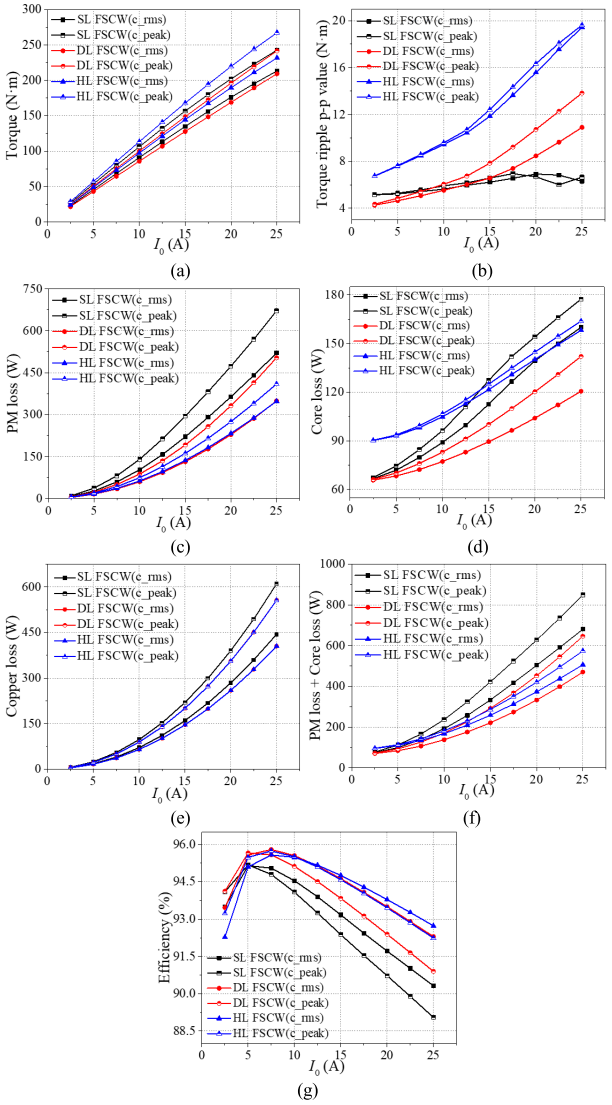

FIGURE 18. Performance comparison between HL FSCW machine and conventional machines. (a) Average torque; (b) Torque ripple; (c) PM loss; (d) Core loss; (e) Copper loss; (f) Summation of PM loss and core loss; (g) Machine efficiency.

For each type of machine, copper loss of constant peak harmonic injection is higher than constant rms harmonic injection, as shown in Fig. 18(e). Copper loss of HL FSCW machine under constant rms and peak harmonic injection are similar with those of DL FSCW machine, and slightly lower than those of SL FSCW machine during the variation of I_0.

When I_0 is relatively high, the summation of PM loss and core loss of SL FSCW machine is the highest under both constant rms and peak harmonic injection, as shown in Fig. 18(f). The summation of the loss of HL FSCW machine with constant rms harmonic injection is higher than that of DL FSCW machine during the variation of I_0. On the contrary, the summation of the loss of HL FSCW machine with constant peak harmonic injection starts to be lower than that of DL FSCW machine after I_0 achieves 15A.

The efficiency of different machines under constant rms and peak harmonic injection are shown in Fig. 18(g), with

PM loss, core loss, and copper loss included in the calculation of efficiency. For each type of machine, machine efficiency of constant peak harmonic injection is higher than efficiency of constant rms harmonic injection when I_0 is relatively low. Then, with the increase of I_0, machine efficiency of constant rms harmonic injection exceeds efficiency of constant peak harmonic injection. Generally, efficiency of HL FSCW machine under both constant rms and peak harmonic injection exceed those of SL and DL FSCW machine when I_0 is relatively high.

Discussions about the influence of machining process on performance of HL FSCW machine are in the Appendix B.

IV. THIRD HARMONIC CURRENT INJECTION OF HL FSCW FIVE-PHASE MACHINE FOR FLUX WEAKENING OPERATION

Third harmonic current injection of 30-slot/24-pole HL FSCW five-phase machine for torque enhancement is analyzed in section III. However, efficiency of HL FSCW machine under constant rms harmonic injection condition (92.73%) is lower than efficiency without harmonic injection (93.55%) when I_0 is equal to 25A. Thus, in the analysis of this section, third harmonic current is not applied to HL FSCW machine in the constant torque operation region using the Maximum Torque Per Ampere (MTPA) strategy. Third harmonic current injection is only applied during flux weakening operation to research the influence of harmonic injection on high speed operation. Since HL FSCW machine analyzed in this paper is designed for wheel-driving application in EVs, the maximum speed is 1400rpm. The frequency of the fundamental current and the third harmonic current at 1400rpm is 280Hz and 840Hz, respectively. Considering control accuracy of current by pulse width modulation (PWM) with conventional Si IGBT devices, it is feasible to inject third harmonic current in flux weakening operation region.

In this paper, 30-slot/24-pole HL FSCW five-phase machine is driven by H-bridge converter for the consideration of more control freedom and better fault-tolerant capacity. Thus, current of each phase can be controlled independently. During constant-torque operation of HL FSCW machine, phase voltage increases with the increase of speed and achieves the limit of DC-link voltage at 700rpm. Negative d_1-axis current is injected under the constraint of constant peak value of phase current due to the current limit of converter during the conventional flux weakening operation. Since q_1-axis current is reduced due to the introduction of d_1-axis current, torque of flux weakening operation declines with the increase of speed.

Third harmonic contained in the back EMF of HL FSCW machine influences the phase voltage under different conditions of both constant torque operation and flux weakening operation. To simplify the analysis, nonlinearity caused by the saturation of stator core and eddy current in rotor is ignored in the calculation of the phase voltage. Besides, since the resistance of each phase is much less than the inductance, resistance is also ignored in the analysis of the phase voltage.

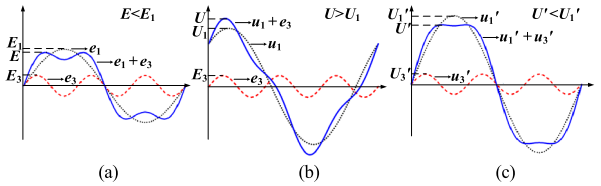

FIGURE 19. Phase voltage of HL FSCW machine under different conditions. (a) No load condition; (b) Conventional flux weakening condition; (c) Flux weakening condition with 3rd harmonic injection.

It is noted that Phase-A is taken as an example, so back EMF, phase current, and voltage mentioned in the following analysis all refer to Phase-A. Other phases in five-phase machine have constant phase angle difference compared with Phase-A, and can be analyzed similarly.

Under no-load condition, since the 1st harmonic in back EMF (e_1) is in phase with the 3rd harmonic in back EMF (e_3), back EMF (e) is reduced by e_3. So the amplitude of back EMF (E) is lower than the amplitude of the 1st harmonic in back EMF (E_1) due to the influence of the amplitude of the 3rd harmonic in back EMF (E_3), as shown in Fig. 19(a).

Phase voltage of conventional flux weakening operation is shown in Fig. 19(b). Different from no-load condition, the 1st harmonic in phase voltage (u_1) is ahead of e_3 because of the influence of the fundamental armature reaction inductance (L_1). Since there is no third harmonic current injection, the 3rd harmonic contained in phase voltage is equal to e_3. The amplitude of phase voltage (U) is higher than the amplitude of the 1st harmonic in phase voltage (U_1) due to the influence of e_3, as shown in Fig. 19(b). The increase of phase voltage caused by e_3 is unfavorable in flux weakening operation, because more d_1-axis current is needed to suppress U_1 to satisfy the limit of DC-link voltage. The increase of d_1-axis current leads to the declination of q_1-axis current, so more torque is sacrificed.

Phase voltage of flux weakening operation with third harmonic current injection is shown in Fig. 19(c). Both d_1-axis and d_3-axis current are injected during flux weakening operation, so the 1st harmonic (u_1') and the 3rd harmonic (u_3') in phase voltage are controlled to be in phase. The relationship of phase angle of u_1' and u_3' are the same as that of e_1 and e_3 under no-load condition. The amplitude of phase voltage (U') is lower than the amplitude of the 1st harmonic in phase voltage (U_1') due to the influence of the amplitude of the 3rd harmonic in phase voltage(U_3'), as shown in Fig. 19(c).

u_1' and u_3' are expressed in (10), where ψ is the phase angle of u_1'; θ is the phase angle of u_3'; ω_e is the electrical angular velocity. i_1' and i_3' are expressed in (11), where α is the phase angle of i_1'; β is the phase angle of i_3'. α indicates the d_1-axis component and q_1-axis component of the 1st harmonic in phase current, as shown in Fig. 20. Similarly, β indicates the d_3-axis component and q_3-axis component of the 3rd harmonic in phase current. α and β are equal to zero during constant-torque operation using the MTPA strategy. With the increase of speed, d_1-axis and d_3-axis current component are increased, so α and β are increased

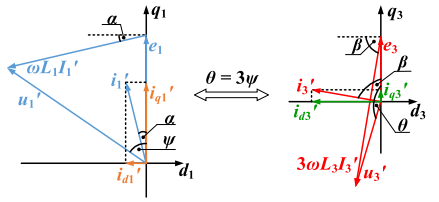

FIGURE 20. Vector graph of phase current and voltage in HL FSCW machine during flux weakening operation with third harmonic current injection.

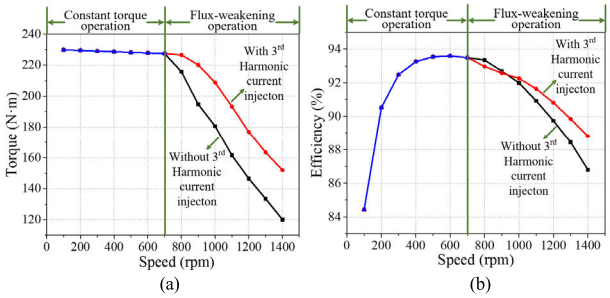

FIGURE 21. (a) Torque speed characteristics of HL FSCW machine with and without 3rd harmonic current injection. (b) Efficiency of HL FSCW machine with and without 3rd harmonic current injection.

as well. The amplitude of i_1' (I_1') and the amplitude of i_3' (I_3') satisfy (12), where I_0 is the amplitude of phase current during constant torque operation and conventional flux weakening operation. So copper loss of flux weakening operation with third harmonic current injection does not exceed copper loss of conventional flux weakening operation. Equation (13) needs to be satisfied to ensure that the relation of phase angles shown in Fig. 19(c) can be achieved.

$$\begin{cases} u_1' = U_1' \sin(\omega_e t + \psi) \\ u_3' = U_3' \sin(3\omega_e t + \theta) \end{cases} \tag{10}$$

$$\begin{cases} i_1' = I_1' \sin(\omega_e t + \alpha) \\ i_3' = I_3' \sin(3\omega_e t + \beta) \end{cases} \tag{11}$$

$$\sqrt{I_1'^2 + I_3'^2} \le I_0 \tag{12}$$

$$\theta = 3\psi \tag{13}$$

Vector graph of phase current and voltage during flux weakening operation with third harmonic current injection is shown in Fig. 20. According to Fig. 20, U_1' and ψ are calculated in (14) according to α and I_1', where L_1 is the fundamental armature reaction inductance (14.53mH). Since θ is determined by ψ in (13), β is calculated according to I_3' and θ in (15). U_3' is also calculated using β and I_3' in (15), where L_3 is the third harmonic armature reaction inductance (14.87mH). Then, phase voltage (u') is calculated by the summation of u_1' and u_3' in (16), and the amplitude of u' (U') is expressed by (17).

$$\begin{cases} U_1' = \sqrt{\left[\omega_e L_1 I_1' \cos(\alpha)\right]^2 + \left[E_1 - \omega_e L_1 I_1' \sin(\alpha)\right]^2} \\ \psi = \arctan \dfrac{\omega_e L_1 I_1' \cos(\alpha)}{E_1 - \omega_e L_1 I_1' \sin(\alpha)} \end{cases} \tag{14}$$

$$\begin{cases} U_3' = \sqrt{\left[3\omega_e L_3 I_3' \cos(\beta)\right]^2 + \left[E_3 - 3\omega_e L_3 I_3' \sin(\beta)\right]^2} \\ \theta = \arctan \dfrac{3\omega_e L_3 I_3' \cos(\beta)}{E_3 - 3\omega_e L_3 I_3' \sin(\beta)} \end{cases} \tag{15}$$

$$u' = u_1' + u_3' = U_1' \sin(\omega_e t + \psi) + U_3' \sin(3\omega_e t + \theta) \tag{16}$$

$$U' = \left(\frac{U_1' + 3U_3'}{3}\right)^{1.5} \cdot \sqrt{\frac{1}{U_3'}} \tag{17}$$

It is noted that since the calculation expressed from (14) to (17) is deduced under the premise that saturation of stator core and eddy current in rotor are ignored, the actual phase current has a certain deviation from the theoretical calculation value. Besides, higher order harmonics (such as the 5th and 7th harmonic) contained in back EMF also influence phase voltage during flux weakening process, which can be controlled by applying harmonic current with the corresponding order. However, harmonic current whose order is higher than 3 is not taken into consideration in the process of current control. It is because current frequency is increased with the increase of speed, and harmonic current with higher order increases the difficulty of current control. Thus, due to the simplicity and ignorance in the theoretical calculation, the amplitude and phase angle of the 1st and 3rd harmonic current for flux weakening operation need to be calibrated according to the theoretical calculation in practical applications. In this paper, the amplitude and phase angle of the 1st and 3rd harmonic current are calibrated according to the simulation results of FEA.

After the theoretical analysis mentioned above, the feasibility of the proposed flux weakening control method with third harmonic current injection is verified by FEA. Compared with conventional flux weakening control method without third harmonic current injection, the proposed method suppresses phase voltage effectively and improves torque significantly during high speed operation, as shown in Fig. 21(a). Therefore, the superiority of flux weakening control method with third harmonic current injection is verified. I_0 is chosen as 25A during both constant-torque operation, flux weakening operation with and without third harmonic current injection. Phase current (i_0) is expressed in (18) for flux weakening operation without third harmonic current injection, where α_0 is the phase angle.

$$i_0 = I_0 \sin(\omega_e t + \alpha_0) \tag{18}$$

Torque is improved significantly after third harmonic current injection during flux weakening operation when speed exceeds 700rpm. Torque at 1400rpm of flux weakening with harmonic injection is 31.77 N·m higher than torque of flux weakening without harmonic injection. Besides, when speed exceeds 1000rpm, machine efficiency of flux weakening with harmonic injection is higher than efficiency of flux weakening without harmonic injection, as shown in Fig. 21(b). Machine losses, including PM loss, core loss, and copper loss, are included in the calculation of efficiency under flux weakening operation with and without harmonic injection.

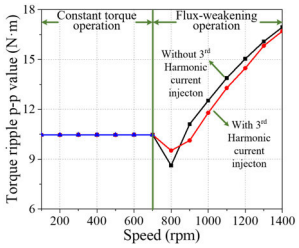

FIGURE 22. Torque ripple of HL FSCW machine with and without third harmonic current injection.

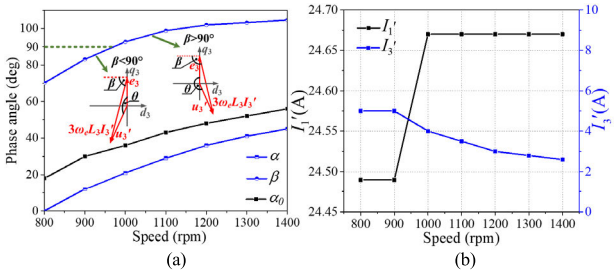

FIGURE 23. (a) Current phase angle comparison of HL FSCW machine during flux weakening operation; (b) Amplitude of phase current in HL FSCW machine during flux weakening operation with third harmonic current injection.

Compared with other losses, mechanical loss is relatively low, which is negligible and not included in the calculation of efficiency. PM loss and core loss are derived from FEA, and copper loss is calculated using analytical method.

Torque ripple comparison between flux weakening operation with and without third harmonic current injection is shown in Fig. 22. Torque ripple increases with the increase of speed for flux weakening region both with and without harmonic injection. When speed exceeds 900rpm, torque ripple of flux weakening with harmonic injection is lower than that of flux weakening without harmonic injection.

Phase angle of i_1' (α) and phase angle of i_3' (β) during flux weakening operation with third harmonic current injection are compared with phase angle of i_0 (α_0), as shown in Fig. 23(a). α is lower than α_0 during the flux weakening process, so torque of flux weakening with harmonic injection is higher than torque of flux weakening without harmonic injection. β exceeds 90° when speed exceeds 1000rpm, which means that negative torque is generated by the 3rd harmonic current to ensure the 3rd harmonic in the phase voltage satisfies (13). However, negative torque caused by 3rd harmonic current is almost negligible, so overall torque is still improved owing to the lower α. The amplitude of i_1' (I_1') and the amplitude of i_3' (I_3') during flux weakening operation with third harmonic current injection are shown in Fig. 23(b).

Finally, it is worth to note that, although the flux weakening control method with third harmonic current injection is proposed for five-phase PMSM and verified by HL FSCW machine in this paper, it can be extended to seven- and nine-phase PMSM to enhance torque during flux weakening operation as well.

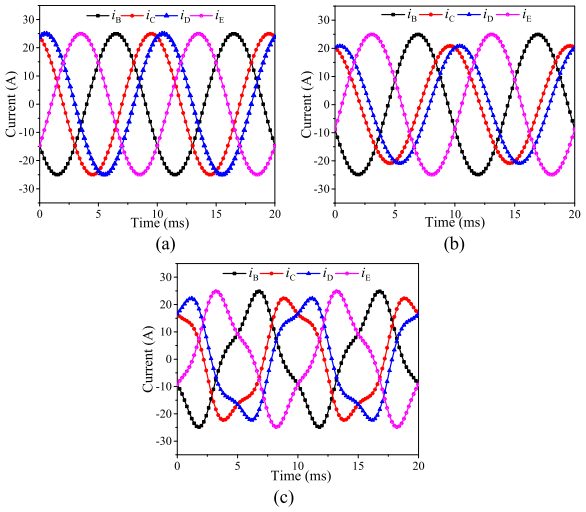

FIGURE 24. Compensatory currents applied to HL FSCW machine. (a) Strategy I. (b) Strategy II. (c) Strategy III.

V. FAULT-TOLERANT STRATEGY OF HL FSCW FIVE-PHASE MACHINE WITH ONE-PHASE OPEN-CIRCUIT FAULT

In this section, fault-tolerant control for HL FSCW five-phase PMSM with one-phase open-circuit fault is investigated. Two compensatory strategies with and without third harmonic current injection are proposed, and compared with the existing compensatory strategy. Since HL FSCW machine is driven by H-bridge converter, compensatory currents in the remaining healthy phases are not constrained by the neutral point.

The first fault-tolerant strategy (Strategy I) is an existing strategy, which is proposed in [18] for five-phase PMSM with one-phase open-circuit fault. Assuming that Phase-A is open-circuit, compensatory currents of remaining healthy phases ($\boldsymbol{i_I}$) are expressed in (19),

$$\boldsymbol{i_I} = \begin{bmatrix} i_B \\ i_C \\ i_D \\ i_E \end{bmatrix} = I_I \begin{bmatrix} \cos(\omega_e t - 54°) \\ \cos(\omega_e t - 162°) \\ \cos(\omega_e t + 162°) \\ \cos(\omega_e t + 54°) \end{bmatrix} \tag{19}$$

where I_I is the amplitude of compensatory currents. Compensatory currents of strategy I are equal-amplitude and sinusoidal as shown in Fig. 24(a), and I_I is equal to 25A. The amplitude of phase current is kept to be same for healthy condition, uncontrolled fault condition, and fault-tolerant condition with strategy I to ensure a fair comparison.

Since phase-to-phase mutual inductance is negligible in HL FSCW machine, electromagnetic torque of fault-tolerant condition with strategy I is calculated in (20),

$$T_e = \frac{(\boldsymbol{e_1} + \boldsymbol{e_3} + \boldsymbol{e_5})\,\boldsymbol{i_I}}{\omega_m}$$
$$\begin{cases} T_e = T_0 + \Delta t \\ \Delta t = t_2 + t_4' + t_4'' + t_6 \end{cases} \tag{20}$$

$$\begin{aligned}\boldsymbol{e_1} &= \begin{bmatrix} e_{\mathrm{B1}} & e_{\mathrm{C1}} & e_{\mathrm{D1}} & e_{\mathrm{E1}} \end{bmatrix} \\ &= E_1 \begin{bmatrix} \cos(\omega_e t - 72°) \\ \cos(\omega_e t - 144°) \\ \cos(\omega_e t + 144°) \\ \cos(\omega_e t + 72°) \end{bmatrix}^{\mathrm{T}} \end{aligned} \tag{21}$$

$$\boldsymbol{e_3} = \begin{bmatrix} e_{\mathrm{B3}} & e_{\mathrm{C3}} & e_{\mathrm{D3}} & e_{\mathrm{E3}} \end{bmatrix} \tag{22}$$

$$\boldsymbol{e_5} = \begin{bmatrix} e_{\mathrm{B5}} & e_{\mathrm{C5}} & e_{\mathrm{D5}} & e_{\mathrm{E5}} \end{bmatrix} \tag{23}$$

where $\boldsymbol{e_1}$, $\boldsymbol{e_3}$, and $\boldsymbol{e_5}$ represent the 1st, 3rd, and 5th harmonic contained in the back EMF of remaining healthy phases, expressed in (21), (22), and (23), respectively. T_e is the electromagnetic torque, which includes the constant component (T_0) and the fluctuated component (Δt). The 2nd harmonic (t_2), the 4th harmonics (t_4' and t_4''), and the 6th harmonic (t_6) are contained in Δt.

T_0 is expressed in (24), with E_1 referring to the amplitude of fundamental harmonic in back EMF. t_2 and t_4' are caused by the 3rd harmonic in back EMF as calculated in (25), whereas t_4'' and t_6 are caused by the 5th harmonic in back EMF as calculated in (26), where E_3 and E_5 are the amplitude of the 3rd and 5th harmonic in back EMF. The influence of higher order harmonics contained in the back EMF of HL FSCW machine is ignored, since amplitudes of harmonics whose orders are higher than 5 are relatively low.

$$\begin{cases} \dfrac{\boldsymbol{e_1 i_I}}{\omega_m} = T_0 \\ T_0 = \dfrac{\sqrt{2}\sqrt{5+\sqrt{5}}}{2} E_1 I_{\mathrm{I}} \end{cases} \tag{24}$$

$$\begin{cases} \dfrac{\boldsymbol{e_3 i_I}}{\omega_m} = t_2 + t_4' = T_2 \cos(2\omega_e t) + T_4' \cos(4\omega_e t) \\ T_2 = \dfrac{\sqrt{2}\sqrt{5-\sqrt{5}}}{8} \left(\sqrt{5}+1\right) E_3 I_{\mathrm{I}} \\ T_4' = \dfrac{\sqrt{2}\sqrt{5+\sqrt{5}}}{8} \left(\sqrt{5}-1\right) E_3 I_{\mathrm{I}} \end{cases} \tag{25}$$

$$\begin{cases} \dfrac{\boldsymbol{e_5 i_I}}{\omega_m} = t_4'' + t_6 = T_4'' \cos(4\omega_e t) + T_6 \cos(6\omega_e t) \\ T_4'' = -\dfrac{\sqrt{5+\sqrt{5}}}{8} \left(3\sqrt{2} - \sqrt{10}\right) E_5 I_{\mathrm{I}} \\ T_6 = -\dfrac{\sqrt{5+\sqrt{5}}}{8} \left(3\sqrt{2} - \sqrt{10}\right) E_5 I_{\mathrm{I}} \end{cases} \tag{26}$$

As analyzed in (25) and (26), the 3rd and 5th harmonic in back EMF leads to the 2nd, 4th, and 6th fluctuating component in torque, which deteriorates fault-tolerant performance of strategy I. Strategy I is proposed for conventional five-phase machine and does not take into consideration of the influence of the 3rd and 5th harmonic in back EMF. However, the 3rd and 5th harmonic in back EMF of 30-slot/24-pole HL FSCW five-phase machine are much higher than conventional five-phase machines of 20-slot/24-pole SL and DL machine. Thus, strategy I is not suitable for compensating one-phase open-circuit fault of HL FSCW machine.

Another compensatory strategy for HL FSCW machine with one-phase open-circuit fault (Strategy II) is proposed in this paper, which includes the influence of the 3rd and 5th harmonic in back EMF. Compensatory currents of strategy II ($\boldsymbol{i_{II}}$) are expressed in (27), and additional current components ($\boldsymbol{i_{a2}}$) are added to the currents of strategy I,

$$\begin{aligned}\boldsymbol{i_{II}} = \boldsymbol{i_I} + \boldsymbol{i_{a2}} &= I_{\mathrm{I}} \begin{bmatrix} \cos(\omega_e t - 54°) \\ \cos(\omega_e t - 162°) \\ \cos(\omega_e t + 162°) \\ \cos(\omega_e t + 54°) \end{bmatrix} \\ &+ I_{a2} \begin{bmatrix} \cos(\omega_e t - \theta_{b2}) \\ \cos(\omega_e t - \theta_{c2}) \\ \cos(\omega_e t - \theta_{d2}) \\ \cos(\omega_e t - \theta_{e2}) \end{bmatrix} \end{aligned} \tag{27}$$

where I_{a2} is the amplitude of $\boldsymbol{i_{a2}}$; θ_{b2}, θ_{c2}, θ_{d2}, and θ_{e2} are the phase angle of the additional current in Phase-B, Phase-C, Phase-D, and Phase-E, respectively. It is noted that $\boldsymbol{i_{a2}}$ has the same frequency compared with $\boldsymbol{i_I}$, so the waveform of $\boldsymbol{i_{II}}$ is sinusoidal with no third harmonic currents included.

Phase angles of additional currents are kept to satisfy (28) for simplifying the analysis.

$$\begin{cases} \theta_{b2} = -\theta_{e2} = \theta_{\alpha 2} \\ \theta_{c2} = -\theta_{d2} = \theta_{\beta 2} \end{cases} \tag{28}$$

$\boldsymbol{i_{a2}}$ interacts with the 1st and 3rd harmonic in back EMF to generate electromagnetic torque as calculated in (29) and (30), where T_{0a} is the constant component in torque; T_{2a}' and T_{2a}'' are the 2nd harmonic in torque; T_{4a} is the 4th harmonic in torque. Since $\boldsymbol{i_{a2}}$ is added to compensate torque ripple of strategy I, equations expressed in (31) need to be satisfied. Then, $\theta_{\alpha 1}$, $\theta_{\beta 2}$, and I_{a2} are obtained by solving (31), which ensures the 2nd and 4th harmonic in torque equal to zero, and maximizes the output torque: $(T_0 + T_{0a})$ at the same time.

$$\begin{cases} \dfrac{\boldsymbol{e_1 i_{a2}}}{\omega_m} = T_{0a} + t_{2a}' = T_{0a} + T_{2a}' \cos(2\omega_e t) \\ T_{0a} = E_1 I_{a2} \left[\cos(\dfrac{2\pi}{5} - \theta_{\alpha 2}) + \cos(\dfrac{4\pi}{5} - \theta_{\beta 2}) \right] \\ T_{2a}' = E_1 I_{a2} \left[\cos(\dfrac{2\pi}{5} + \theta_{\alpha 2}) + \cos(\dfrac{4\pi}{5} + \theta_{\beta 2}) \right] \end{cases} \tag{29}$$

$$\begin{cases} \dfrac{\boldsymbol{e_3 i_{a2}}}{\omega_m} = t_{2a}'' + t_{4a} = T_{2a}'' \cos(2\omega_e t) + T_{4a} \cos(4\omega_e t) \\ T_{2a}'' = -E_3 I_{a2} \left[\cos(\dfrac{4\pi}{5} + \theta_{\alpha 2}) + \cos(\dfrac{2\pi}{5} - \theta_{\beta 2}) \right] \\ T_{4a} = -E_3 I_{a2} \left[\cos(\dfrac{4\pi}{5} - \theta_{\alpha 2}) + \cos(\dfrac{2\pi}{5} + \theta_{\beta 2}) \right] \end{cases} \tag{30}$$

$$\begin{cases} \mathrm{Max}\,[T_0 + T_{0a}] \\ T_{2a}' + T_{2a}'' + T_2 = 0 \\ T_{4a} + T_4' + T_4'' = 0 \end{cases} \tag{31}$$

Therefore, compensatory currents of strategy II are obtained as in (32).

$$\boldsymbol{i_{II}} = 29 \begin{bmatrix} \cos(\omega_e t - 54°) - 0.286\cos(\omega_e t - 0.9°) \\ \cos(\omega_e t - 162°) - 0.286\cos(\omega_e t - 153.2°) \\ \cos(\omega_e t + 162°) - 0.286\cos(\omega_e t + 153.2°) \\ \cos(\omega_e t + 54°) - 0.286\cos(\omega_e t + 0.9°) \end{bmatrix} \tag{32}$$

Compensatory currents of strategy II are sinusoidal, but amplitudes of currents are unequal, which is different from strategy I, as shown in Fig. 24(b). The amplitudes of currents in Phase-B and Phase-E are the same (25A), which is higher than the amplitudes of currents in Phase-C and Phase-D (20.85A). The maximum of compensatory currents of strategy II is kept to be 25A to ensure a fair comparison with strategy I.

To investigate the influence of third harmonic currents on fault-tolerant performance, the third compensatory strategy (Strategy III) for HL FSCW machine with one-phase open-circuit fault is proposed in this paper. Compensatory currents of strategy III ($\boldsymbol{i_{III}}$) are expressed in (33), which substitutes $\boldsymbol{i}_{a2}$ with third harmonic additional current components ($\boldsymbol{i}_{a3}$).

$$\boldsymbol{i_{III}} = \boldsymbol{i_I} + \boldsymbol{i}_{a3} = I_I \begin{bmatrix} \cos(\omega_e t - 54°) \\ \cos(\omega_e t - 162°) \\ \cos(\omega_e t + 162°) \\ \cos(\omega_e t + 54°) \end{bmatrix} + I_{a3} \begin{bmatrix} \cos(3\omega_e t - \theta_{b3}) \\ \cos(3\omega_e t - \theta_{c3}) \\ \cos(3\omega_e t - \theta_{d3}) \\ \cos(3\omega_e t - \theta_{e3}) \end{bmatrix} \tag{33}$$

where I_{a3} is the amplitude of $\boldsymbol{i}_{a3}$; θ_{b3}, θ_{c3}, θ_{d3}, and θ_{e3} are the phase angle of the additional current in Phase-B, Phase-C, Phase-D, and Phase-E, respectively. Similar with strategy II, phase angles of $\boldsymbol{i_{a3}}$ are kept to satisfy (34).

$$\begin{cases} \theta_{b3} = -\theta_{e3} = \theta_{\alpha 3} \\ \theta_{c3} = -\theta_{d3} = \theta_{\beta 3} \end{cases} \tag{34}$$

$\boldsymbol{i}_{a3}$ interacts with the 1st and 3rd harmonic in back EMF to generate electromagnetic torque as calculated in (35) and (36), where T_{0t}, T_{2t}, T_{4t}, and T_{6t} represent the constant component, the 2nd, 4th, and 6th harmonic in torque, respectively. Similar with strategy II, phase angles of compensatory currents should satisfy torque equations in (37), which maximizes the output torque: $(T_0 + T_{0t})$ and suppresses the 2nd and 4th fluctuating component in torque.

$$\begin{cases} \dfrac{\boldsymbol{e_1 i_{a3}}}{\omega_m} = t_{2t} + t_{4t} = T_{2t}\cos(2\omega_e t) + T_{4t}\cos(4\omega_e t) \\ T_{2t} = E_1 I_{a3}\left[\cos(\dfrac{2\pi}{5} - \theta_{\alpha 3}) + \cos(\dfrac{4\pi}{5} - \theta_{\beta 3})\right] \\ T_{4t} = E_1 I_{a3}\left[\cos(\dfrac{2\pi}{5} + \theta_{\alpha 3}) + \cos(\dfrac{4\pi}{5} + \theta_{\beta 3})\right] \end{cases} \tag{35}$$

$$\begin{cases} \dfrac{\boldsymbol{e_3 i_{a3}}}{\omega_m} = T_{0t} + t_{6t} = T_{0t} + T_{6t}\cos(6\omega_e t) \\ T_{0t} = -E_3 I_{a3}\left[\cos(\dfrac{4\pi}{5} + \theta_{\alpha 3}) + \cos(\dfrac{2\pi}{5} - \theta_{\beta 3})\right] \\ T_{6t} = -E_3 I_{a3}\left[\cos(\dfrac{4\pi}{5} - \theta_{\alpha 3}) + \cos(\dfrac{2\pi}{5} + \theta_{\beta 3})\right] \end{cases} \tag{36}$$

$$\begin{cases} \text{Max}\,[T_0 + T_{0t}] \\ T_{2t} + T_2 = 0 \\ T_{4t} + T_4' + T_4'' = 0 \end{cases} \tag{37}$$

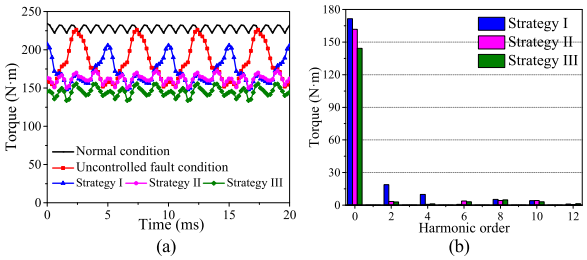

FIGURE 25. (a) Torque comparison of HL FSCW machine under different conditions; (b) Harmonic analysis of torque generated by HL FSCW machine under fault-tolerant condition with strategy I, II, and III.

Then, compensatory currents of strategy III are obtained as expressed in (38).

$$\boldsymbol{i_{III}} = 21.5 \begin{bmatrix} \cos(\omega_e t - 54°) - 0.182\cos(3\omega_e t - 29.9°) \\ \cos(\omega_e t - 162°) - 0.182\cos(3\omega_e t + 173.1°) \\ \cos(\omega_e t + 162°) - 0.182\cos(3\omega_e t - 173.1°) \\ \cos(\omega_e t + 54°) - 0.182\cos(3\omega_e t + 29.9°) \end{bmatrix} \tag{38}$$

Compensatory currents of strategy III are non-sinusoidal and unequal-amplitude, as shown in Fig. 24(c). The amplitudes of currents in Phase-B and Phase-E are the same (25A), which is higher than the amplitudes of currents in Phase-C and Phase-D (22.29A). The maximum of compensatory currents in strategy III is also kept to be 25A to ensure a fair comparison with strategy I and II.

Torque of normal condition, uncontrolled fault condition, and fault-tolerant condition with strategy I, II, and III are compared in Fig. 25(a). Although torque ripple of strategy I is lower than that of uncontrolled fault condition, torque ripple of strategy I is still high compared with that of normal condition. Torque ripple of fault-tolerant condition with strategy II and III are both much lower than that of strategy I, and average torque of strategy II and III are also lower than that of strategy I. Harmonic analysis of torque under fault-tolerant condition with strategy I, II, and III is shown in Fig. 25(b). The 2nd and 4th harmonic are contained in the torque of strategy I, which consists with the theoretical analysis mentioned above and results in intolerable high torque ripple. For strategy II and III, the 2nd and 4th harmonic in torque are suppressed effectively by additional currents of $\boldsymbol{i}_{a2}$ and $\boldsymbol{i}_{a3}$, respectively.

Although average torque of strategy II (0.71 p.u.) is declined slightly compared with strategy I (0.75 p.u.), as listed in Table 5, torque ripple of strategy II (2.98 p.u.) is much lower than that of strategy I (7.35 p.u.). Torque ripple of strategy II (2.98 p.u.) and strategy III (2.92 p.u.) are similar, but average torque of strategy II (0.71 p.u.) is higher than that of strategy III (0.63 p.u.).

Losses and efficiency of HL FSCW machine under different conditions are listed in Table 6. Efficiency of strategy II is the highest among the three strategies, with core loss, PM loss, and copper loss taken into consideration in the calculation of efficiency. Therefore, strategy II, with unequal-amplitude sinusoidal compensatory currents, is superior to

TABLE 5. Torque of HL FSCW machine under different conditions.

Case	Torque (N·m)	Torque (p.u.)	Torque ripple (%)	Torque ripple (p.u.)
(a) [1]	228.20	1	4.59	1
(b) [2]	182.77	0.80	40.63	8.85
(c) [3]	171.43	0.75	33.72	7.35
(d) [4]	161.75	0.71	13.68	2.98
(e) [5]	144.23	0.63	13.39	2.92

[1]Case (a): normal condition. [2]Case (b): uncontrolled fault condition. [3]Case (c): fault-tolerant condition with strategy I. [4]Case (d): fault-tolerant condition with strategy II. [5]Case (e): fault-tolerant condition with strategy III.

TABLE 6. Losses and efficiency of HL FSCW machine under different conditions.

Case	Core loss (W)	PM loss (W)	Copper loss (W)	Efficiency (%)
(a) [1]	133.88	258.15	405.25	93.55
(b) [2]	124.23	201.60	324.25	93.43
(c) [3]	121.84	194.77	324.25	93.11
(d) [4]	117.75	167.76	273.56	93.61
(e) [5]	96.31	165.15	247.74	93.47

[1]Case (a): normal condition. [2]Case (b): uncontrolled fault condition. [3]Case (c): fault-tolerant condition with strategy I. [4]Case (d): fault-tolerant condition with strategy II. [5]Case (e): fault-tolerant condition with strategy III.

strategy I with equal-amplitude sinusoidal compensatory currents and strategy III with third harmonic current injection. It is proved that third harmonic injection does not have advantages during fault-tolerant operation of HL FSCW machine, and performance of HL FSCW machine with one-phase open-circuit fault is improved by applying strategy II.

VI. CONCLUSION

(1) Harmonic content in the synthesized MMF of 30-slot/24-pole HL FSCW machine is different from that of 20-slot/24-pole SL and DL FSCW machine due to the change of winding configuration.

(2) Winding factor of the 36th harmonic of HL FSCW machine achieves the maximum of 1 as the working harmonic (the 12th harmonic). Thus, HL FSCW five-phase machine is more suitable than 20-slot/24-pole SL and DL FSCW machine for third harmonic injection to improve torque.

(3) Compared with flux weakening operation without harmonic injection, torque and efficiency are improved during flux weakening operation with third harmonic current injection, which is validated by FEA with nonlinearity and higher order harmonics in back EMF taken into consideration.

(4) Two compensatory strategies are proposed for HL FSCW machine with one-phase open-circuit fault, which suppresses the 2nd and 4th torque ripple effectively. Compared with strategy III with third harmonic current injection, strategy II with unequal-amplitude sinusoidal compensatory currents generates higher torque under fault-tolerant condition.

TABLE 7. Introductions of FEM.

Software	Maxwell
Solver	Maxwell-2D: Transient Magnetic Solver
Boundary conditions	Vector Potential Boundary
Governing equations [1]	$\nabla\times\upsilon\nabla\times A=J_s-\sigma\frac{dA}{dt}-\sigma\nabla V+\nabla\times H_c$

[1]A is the magnetic vector potential; υ is the reluctivity; J_s is the source current density; V is the electric potential; H_c is the coercivity of the permanent magnet.

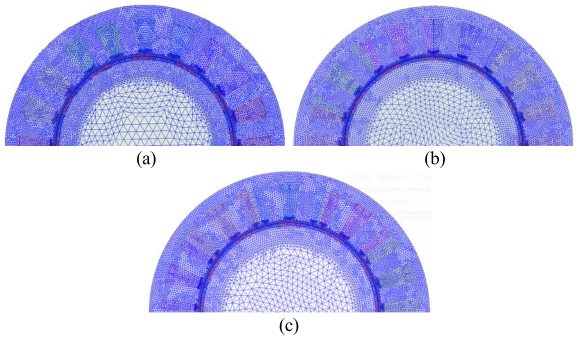

FIGURE 26. Mesh plots of different machines. (a) 20-slot/24-pole SL FSCW machine; (b) 20-slot/24-pole DL FSCW machine; (c) 30-slot/24-pole HL FSCW machine.

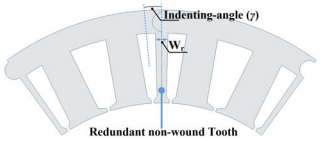

FIGURE 27. The width of the redundant non-wound tooth.

APPENDIX A

Introductions of FEM used for analyses of SL, DL, and HL FSCW machine are listed in Table 7, including software, solver, boundary conditions, and governing equations. Mesh plots of different machines are shown in Fig. 26.

PMs used in SL, DL, and HL FSCW machine are N52H, which is radially magnetized. The conductivity of N52H is 714290 siemens/m; the remanence of N52H is 1.32 T at 90°; the coercivity of N52H is −650 kA/m at 90°.

APPENDIX B

For HL FSCW machine, the complex structure and errors in machining process may lead to a certain degree of performance degradation, but the advantages of HL FSCW machine over DL FSCW machine will be maintained.

It is undeniable that, if the indenting-angle (γ) which is related with the width of the redundant non-wound tooth (W_r) is not exactly equal to 3°, as shown in Fig. 27, due to the poor machining accuracy of redundant non-wound teeth, machine performance will be influenced. If the actual value of indenting angle (γ') is slightly higher or lower than the design value of indenting angle (γ=3°), the winding factors of the 2nd and 8th harmonic are still suppressed in HL FSCW machine, as shown in Fig. 28. Compared with the 12th harmonic, the winding factor of the 36th harmonic

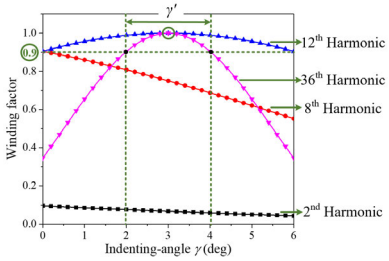

FIGURE 28. The winding factors of different harmonics considering the machining errors of γ'.

decreases faster when γ' is higher or lower than 3°. But, fortunately, when γ' is between 2° and 4°, the winding factor of the 36th harmonic is higher than 0.9, and the decrease of the winding factor of the 12th harmonic is negligible. Therefore, the harmonics which have important effects on the performance of HL FSCW machine are only changed slightly. The advantages of HL FSCW machine brought by higher 12th and 36th harmonic and lower 2nd and 8th harmonic will not be lost although γ' may not be exactly equal to 3° due to machining errors.

REFERENCES

[1] S. Dwari and L. Parsa, "An optimal control technique for multiphase PM machines under open-circuit faults," *IEEE Trans. Ind. Electron.*, vol. 55, no. 5, pp. 1988–1995, May 2008.
[2] E. Levi, "Multiphase electric machines for variable-speed applications," *IEEE Trans. Ind. Electron.*, vol. 55, no. 5, pp. 1893–1909, May 2008.
[3] L. Parsa and H. A. Toliyat, "Fault-tolerant interior-permanent-magnet machines for hybrid electric vehicle applications," *IEEE Trans. Veh. Technol.*, vol. 56, no. 4, pp. 1546–1552, Jul. 2007.
[4] F. Scuiller, "Third harmonic current injection to reduce the pulsating torque of a five-phase SPM machine," in *Proc. 41st Annu. Conf. IEEE Ind. Electron. Soc. (IECON)*, Yokohama, Japan, Nov. 2015, pp. 000811–000816.
[5] W. Cao, B. C. Mecrow, G. J. Atkinson, J. W. Bennett, and D. J. Atkinson, "Overview of electric motor technologies used for more electric aircraft (MEA)," *IEEE Trans. Ind. Electron.*, vol. 59, no. 9, pp. 3523–3531, Sep. 2012.
[6] K. Wang, Z. Q. Zhu, and G. Ombach, "Torque enhancement of surface-mounted permanent magnet machine using third-order harmonic," *IEEE Trans. Magn.*, vol. 50, no. 3, pp. 104–113, Mar. 2014.
[7] L. Parsa and H. A. Toliyat, "Five-phase permanent-magnet motor drives," *IEEE Trans. Ind. Appl.*, vol. 41, no. 1, pp. 30–37, Jan. 2005.
[8] M. Slunjski, M. Jones, and E. Levi, "Control of a symmetrical nine-phase PMSM with highly non-sinusoidal back-electromotive force using third harmonic current injection," in *Proc. 45th Annu. Conf. IEEE Ind. Electron. Soc. (IECON)*, Lisbon, Portugal, Oct. 2019, pp. 969–974.
[9] M. Slunjski, O. Stiscia, M. Jones, and E. Levi, "General torque enhancement approach for a nine-phase surface PMSM with built-in fault tolerance," *IEEE Trans. Ind. Electron.*, early access, Jul. 10, 2020, doi: 10.1109/TIE.2020.3007053.
[10] K. Wang, D. S. Lin, P. Zhou, Z. Q. Zhu, and S. Zhang, "Analytical determination of 3rd order harmonic current into five phase PM machine for maximum torque," in *Proc. IEEE Int. Electr. Mach. Drives Conf. (IEMDC)*, Coeur d'Alene, ID, USA, May 2015, pp. 630–636.
[11] Z. Y. Gu, K. Wang, Z. Q. Zhu, Z. Z. Wu, C. Liu, and R. W. Cao, "Torque improvement in five-phase unequal tooth SPM machine by injecting third harmonic current," *IEEE Trans. Veh. Technol.*, vol. 67, no. 1, pp. 206–215, Jan. 2018.
[12] Z. Y. Gu, K. Wang, Z. Q. Zhu, and C. Liu, "Torque improvement utilizing third harmonic current in five-phase PM machines with unequal tooth," in *Proc. IEEE Vehicle Power Propuls. Conf. (VPPC)*, Hangzhou, China, Oct. 2016, pp. 1–5.
[13] K. Wang, Z. Y. Gu, C. Liu, and Z. Q. Zhu, "Design and analysis of a five-phase SPM machine considering third harmonic current injection," *IEEE Trans. Energy Convers.*, vol. 33, no. 3, pp. 1108–1117, Sep. 2018.
[14] K. Wang, Z. Q. Zhu, and G. Ombach, "Torque improvement of five-phase surface-mounted permanent magnet machine using third-order harmonic," *IEEE Trans. Energy Convers.*, vol. 29, no. 3, pp. 735–747, Sep. 2014.
[15] Z. Gu, K. Wang, R. Cao, and C. Liu, "Design of five phase SPM machine considering third harmonic current injection," in *Proc. 19th Int. Conf. Elect. Mach. Syst. (ICEMS)*, Chiba, Japan, Nov. 2016, pp. 1–5.
[16] Y. Chen and B. Liu, "Design and analysis of a five-phase fault-tolerant permanent magnet synchronous motor for aerospace starter-generator system," *IEEE Access*, vol. 7, pp. 135040–135049, 2019.
[17] M. Farshadnia, M. A. Masood Cheema, A. Pouramin, R. Dutta, and J. E. Fletcher, "Design of optimal winding configurations for symmetrical multiphase concentrated-wound surface-mount PMSMs to achieve maximum torque density under current harmonic injection," *IEEE Trans. Ind. Electron.*, vol. 65, no. 2, pp. 1751–1761, Feb. 2018.
[18] Y. Sui, P. Zheng, Z. Yin, M. Wang, and C. Wang, "Open-circuit fault-tolerant control of five-phase PM machine based on reconfiguring maximum round magnetomotive force," *IEEE Trans. Ind. Electron.*, vol. 66, no. 1, pp. 48–59, Jan. 2019.
[19] Y. Sui, P. Zheng, F. Wu, B. Yu, P. Wang, and J. Zhang, "Research on a 20-slot/22-pole five-phase fault-tolerant PMSM used for four-wheel-drive electric vehicles," *Energies*, vol. 7, no. 3, pp. 1265–1287, Mar. 2014.
[20] S. Dwari and L. Parsa, "Open-circuit fault tolerant control of five-phase permanent magnet motors with third-harmonic back-EMF," in *Proc. 34th Annu. Conf. IEEE Ind. Electron.*, Orlando, FL, USA, Nov. 2008, pp. 3114–3119.
[21] S. Dwari and L. Parsa, "Fault-tolerant control of five-phase permanent-magnet motors with trapezoidal back EMF," *IEEE Trans. Ind. Electron.*, vol. 58, no. 2, pp. 476–485, Feb. 2011.
[22] A. Mohammadpour and L. Parsa, "A unified fault-tolerant current control approach for five-phase PM motors with trapezoidal back EMF under different stator winding connections," *IEEE Trans. Power Electron.*, vol. 28, no. 7, pp. 3517–3527, Jul. 2013.
[23] T. M. Jahns, "Flux-weakening regime operation of an interior permanent-magnet synchronous motor drive," *IEEE Trans. Ind. Appl.*, vol. IA-23, no. 4, pp. 681–689, Jul. 1987.
[24] L. Parsa, N. Kim, and H. A. Toliyat, "Field weakening operation of high torque density five-phase permanent magnet motor drives," in *Proc. IEEE Int. Conf. Electr. Mach. Drives*, San Antonio, TX, USA, May 2005, pp. 1507–1512.
[25] S. Xuelei, W. Xuhui, and C. Wei, "Research on field-weakening control of multiphase permanent magnet synchronous motor," in *Proc. Int. Conf. Electr. Mach. Syst.*, Beijing, China, Aug. 2011, pp. 1–5.
[26] H. Zahr, J. Gong, E. Semail, and F. Scuiller, "Comparison of optimized control strategies of a high-speed traction machine with five phases and bi-harmonic electromotive force," *Energies*, vol. 9, no. 12, p. 952, Nov. 2016.
[27] J. Gong, H. Zahr, E. Semail, M. Trabelsi, B. Aslan, and F. Scuiller, "Design considerations of five-phase machine with double p/3p polarity," *IEEE Trans. Energy Convers.*, vol. 34, no. 1, pp. 12–24, Mar. 2019.
[28] B. Aslan and E. Semail, "New 5-phase concentrated winding machine with bi-harmonic rotor for automotive application," in *Proc. Int. Conf. Electr. Mach. (ICEM)*, Berlin, Germany, Sep. 2014, pp. 2114–2119.
[29] H. Zahr, E. Semail, B. Aslan, and F. Scuiller, "Maximum torque per ampere strategy for a biharmonic five-phase synchronous machine," in *Proc. Int. Symp. Power Electron., Electr. Drives, Autom. Motion (SPEEDAM)*, Anacapri, Italy, Jun. 2016, pp. 91–97.
[30] F. Scuiller and E. Semail, "Inductances and back-emf harmonics influence on the torque/speed characteristic of five-phase SPM machine," in *Proc. IEEE Vehicle Power Propuls. Conf. (VPPC)*, Coimbra, Portugal, Oct. 2014, pp. 1–6.
[31] F. Scuiller, H. Zahr, and E. Semail, "Maximum reachable torque, power and speed for five-phase SPM machine with low armature reaction," *IEEE Trans. Energy Convers.*, vol. 31, no. 3, pp. 959–969, Sep. 2016.

JIAXUAN HUANG was born in Inner Mongolia, China, in 1996. She received the B.Sc. degree in electrical engineering from the Harbin Institute of Technology, Harbin, China, in 2018, where she is currently pursuing the Ph.D. degree in electrical engineering with the School of Electrical Engineering and Automation. Her current research interests include design and control of multiphase permanent-magnet synchronous machine.

PING ZHENG (Senior Member, IEEE) received the B.Sc., M.Sc., and Ph.D. degrees from the Harbin Institute of Technology, Harbin, China, in 1992, 1995, and 1999, respectively, all in electrical engineering. Since 1995, she has been with the Harbin Institute of Technology, where she has been a Professor, since 2005. She is the author or coauthor of more than 270 published refereed technical papers and four books. She is the holder of 70 Chinese invention patents. Her current research interests include electric machines and control, hybrid electric vehicles, and the cloud computing of electric machine systems.

Dr. Zheng was a recipient of more than 30 technical awards, including the "China Youth Science and Technology Award" from the Organization Department of the Communist Party of China in 2009, the "National Science Foundation for Distinguished Young Scholars of China" from the National Natural Science Foundation of China in 2013, the "Chang Jiang Scholar Professor" from the Ministry of Education of China in 2014, and the "National High-Level Talent Special Support Program" from the Organization Department of the Communist Party of China in 2016.

YI SUI (Member, IEEE) was born in Jilin, China, in 1987. He received the B.Sc., M.Sc., and Ph.D. degrees from the Harbin Institute of Technology, Harbin, China, in 2009, 2011, and 2016, respectively, all in electrical engineering. Since 2016, he has been with the Harbin Institute of Technology. His current research interests include fault-tolerant permanent-magnet synchronous machines and permanent-magnet linear machines.

JIGUI ZHENG received the B.Sc. degree in mechatronic engineering from the Jilin University of Technology, Changchun, China, in 2001, the M.Sc. degree from the Beijing University of Aeronautics and Astronautics, Beijing, China, in 2009, and the Ph.D. degree in electrical engineering from the Harbin Institute of Technology, Harbin, China, in 2018. Since 2001, he has been with the R&D Center, Beijing Institute of Precise Mechatronics and Controls, where he has been a Professor, since 2016. He is the author or coauthor of more than 70 published refereed technical papers and two books. He is the holder of 80 Chinese invention patents. His current research interests include space electromechanical servo system technology, machine, and control.

Dr. Zheng was a recipient of more than 20 technical awards, including "China Aerospace Science and Technology Corporation Award", "China Academy of Launch Vehicle Technology Award", and "National Defense Science and Technology Award". He is also a member of intelligent manufacturing group of Science and Technology Committee.

ZUOSHENG YIN was born in Heilongjiang, China, in 1994. He received the B.Sc. and M.Sc. degrees in electrical engineering from the Harbin Institute of Technology, Harbin, China, in 2016 and 2018, respectively, where he is currently pursuing the Ph.D. degree in electrical engineering. His current research interests include design and control of multiphase fault-tolerant permanent-magnet machine.

LUMING CHENG received the B.Sc. degree in electrical engineering from the Harbin Institute of Technology, Harbin, China, in 2013, where he is currently pursuing the Ph.D. degree in electrical engineering with the School of Electrical Engineering and Automation. His current research interests include design and post-fault control of multiphase fault-tolerant permanent-magnet machines and drives.